Petroleum Science 21 (2024) 3692–3705

Contents lists available at ScienceDirect

Petroleum Science

journal homepage: www.keaipublishing.com/en/journals/petroleum-science

Original Paper

Nitrogen isotopes of marine oils in the Tarim Basin, China: Implications for the origin of organic matters and the paleoenvironment

Yang Bai [a, b], Jian-Fa Chen [a, b, *], Wen-Zhe Gang [a, b], Xin-Jian Zhu [c], Václav Suchý [d], Shuai-Qi Tang [a, b], Jin Wu [a, b], Min Li [e], Sheng-Bao Shi [a]

[a] National Key Laboratory of Petroleum Resources and Engineering, China University of Petroleum (Beijing), Beijing, 102249, China
[b] College of Geoscience, China University of Petroleum (Beijing), Beijing, 102249, China
[c] PetroChina Hangzhou Research Institute of Geology, Hangzhou, 310023, Zhejiang, China
[d] Nuclear Physics Institute, v. v. i., Academy of Sciences of the Czech Republic, Na Truhlárce 39/64, 180 86 Prague 8, Czech Republic
[e] Chinese Academy of Geological Sciences, Beijing, 100037, China

ARTICLE INFO

Article history:
Received 16 January 2024
Received in revised form
27 March 2024
Accepted 22 May 2024
Available online 23 May 2024

Edited by Jie Hao

Keywords:
Nitrogen isotope
Nitrogenous components
Crude oils
Organic matter
Redox conditions
Nitrogen cycle

ABSTRACT

Nitrogen isotope compositions ($\delta^{15}N$) of sedimentary rocks are usually used to reconstruct the paleoenvironment and nitrogen (N) biogeochemical cycle. The $\delta^{15}N$ values of crude oils inherit the characteristics of relevant source rocks and can well reflect the information of hydrocarbon-forming organisms and environment in ancient water column. However, studies on the $\delta^{15}N$ of crude oils are limited due to the low N content. In this study, a new efficient method is applied to the marine oils from the Bashituo (BST) and Halahatang (HLHT) areas of the Tarim Basin to obtain the nitrogenous components (i.e., nonhydrocarbons and asphaltenes) for the achievement of N concentration. The carbon and nitrogen isotopes of these components and the biomarkers of oils were measured. The $\delta^{15}N$ values in asphaltenes ($\delta^{15}N_{Asp}$) are significantly heavier than those in nonhydrocarbons ($\delta^{15}N_{NSOs}$) in these oils, which are attributed to the potential directional N transfer and kinetic isotope fractionation during the thermal evolution of organic matters (OM). The $\delta^{15}N_{Asp}$ values have significant correlations with OM origin associated parameters and weak correlations with environmental parameters, suggesting that the difference in $\delta^{15}N_{Asp}$ values is mainly resulted from biological source rather than redox conditions. The $\delta^{15}N_{NSOs}$ values have a closer relationship with the redox condition than biological characteristics, indicating that they have a good response to paleoenvironmental variation in the water column, which is not completely overprinted by the difference of OM origin. Different redox conditions give rise to distinct nitrogen cycles, resulting in various $\delta^{15}N$ values. Anammox occurs in the water column of the Early Cambrian dominated by physically stratified conditions with significant isotope fractionation, resulting in relatively heavier $\delta^{15}N$ of OM in the BST area. In the Middle–Late Ordovician period, the limited suboxic zone leads to an insignificant positive bias of $\delta^{15}N$ caused by partial denitrification in the HLHT oils. The evaluation of $\delta^{15}N$ in nitrogenous fractions enables a more comprehensive reconstruction of N cycle for ancient oceans.

1. Introduction

Nitrogen (N), one of the vital elements of life on earth, exists in marine environments as bioavailable forms of dissolved N_2, ammonium (NH_4^+), nitrite (NO_2^-), nitrate (NO_3^-) and dissolved organic nitrogen (DON) (Gruber and Galloway, 2008; Canfield et al., 2010; Ader et al., 2016). Their contents depend on the redox conditions of seawater, and have significant effects on marine primary productivity and N-biogeochemical cycle (Tyrrell, 1999; Gruber and Galloway, 2008; Canfield et al., 2010; Godfrey et al., 2013; Wang et al., 2015; Stüeken et al., 2016). The differential consumption of various forms of N by organisms in different water environments will lead to the differences in nitrogen isotope compositions ($\delta^{15}N$) of organisms and residual N in water columns (Chen et al., 2020).

* Corresponding author. National Key Laboratory of Petroleum Resources and Engineering, China University of Petroleum (Beijing), Beijing, 102249, China.
E-mail address: jfchen@cup.edu.cn (J.-F. Chen).

https://doi.org/10.1016/j.petsci.2024.05.016

Research on N exchange between the water column and sediments also suggest that the $\delta^{15}N$ of sediments can indicate the predominant N metabolism in the water column, and reveal the isotopic balance between various N sources (including external atmospheric N_2 and internal NO_3^- and NH_4^+) and organisms (Miyake and Wada, 1967; Altabet and Francois, 1994; Baxby et al., 1994; Sigman and Casciotti, 2009; Chen et al., 2019). Therefore, the $\delta^{15}N$ in sediments is always regarded as an effective indicator for documenting the original marine biological and paleoenvironmental information, and it is widely used to reconstruct the N biogeochemical cycle (Quan et al., 2008, 2013; Cremonese et al., 2013; Chen et al., 2019; Kędra et al., 2019; Quan and Adeboye, 2021).

Current study on $\delta^{15}N$ is mainly concentrated on sedimentary rocks, whereas the similar study on crude oils is still restricted by the lack of appropriate analytical methods (Hoering and Moore, 1958; Quan et al., 2013; Ader et al., 2016; Chen et al., 2019). The low N content (usually $\leq$2 wt%) and high C/N ratio in oils result in the inaccuracy of N isotopic testing data (Tissot and Welte, 1984; Prado et al., 2017; Silva et al., 2020). However, it cannot be ignored that N isotopes can preserve more original geological information for high-maturity oils than other geochemical parameters (Baxby et al., 1994; Ader et al., 2006; 2016; Chen et al., 2023). Therefore, one arising question is how to employ $\delta^{15}N$ in oils to reveal the original characteristics of sedimentary water column.

N in oils is mainly accumulated in nonhydrocarbons (NSOs) and asphaltenes, and only very little in aromatic hydrocarbons (Oldenburg et al., 2014; Prado et al., 2017). NSOs and asphaltenes, intermediate products of hydrocarbon generation during thermal evolution, serve as bridge roles, revealing the genetic mechanisms of hydrocarbons (Li et al., 2001; Rashid et al., 2019; Wu et al., 2020). They contain porphyrin and other organic N compounds, which originate from organic matters (OM), such as plankton, algae, bacteria, and higher plants (Zhang et al., 2020). In addition, it has been proven that the contents of some nitrogenous components are significantly related to the paleoenvironment (Zhang et al., 2020). Thus, the N isotope signals of nitrogenous components may be able to replace those of crude oils, and theoretically offer fresh perspectives and opportunities to study the biological and paleoenvironmental characteristics.

It has been widely accepted that the Lower Paleozoic marine strata in the Tarim Basin are rich in oil and gas resources, and the studies of source rocks and oils are of great significance for deep and ultra-deep exploration (Zhu et al., 2019a,b; Li et al., 2020; Liu et al., 2022). However, due to the relatively high degree of thermal evolution caused by deep burial of strata, the geochemical indicators with poor thermal stability have been affected (Bao et al., 2018). Hence, the concluded biological and environmental characteristics are always discrepant resulting from different indicators (Li et al., 2020; Su et al., 2020; Song et al., 2019; Tang et al., 2019). In this case, N isotopes with strong thermal stability exhibit significant advantages in recording original geological information (Williams et al., 1995; Schimmelmann and Lis, 2010; Ader et al., 2016). In the past decades, despite the rise of N isotope research, the relevant study on Lower Paleozoic source rocks in the Tarim Basin is limited, which is mainly caused by the lack of accurate detection methods and samples collecting from deep strata. The related study has only been reported in Su et al. (2020), which shows that the $\delta^{15}N$ values of the Lower Cambrian source rocks of Keping outcrop in western Tarim Basin varied over the range of −4.0‰–4.0‰, those of the Upper Cambrian source rocks in the Tadong uplift were in the range of −2.0‰–5.0‰, and those of the Upper Ordovician source rocks ranged from 2.0‰ to 10.0‰. Therefore, there are significant differences in the distribution of $\delta^{15}N$ in different layers of the Lower Paleozoic source rocks in the Tarim Basin, and the data is insufficient. Moreover, the study about the $\delta^{15}N$ of crude oils in the Tarim Basin is rare, which remains to be further explored.

This study addressed the current lack of inaccurate detection of $\delta^{15}N$ in low-N crude oil, and put forward the application prospect of $\delta^{15}N$ in nitrogenous components. In this paper, the values of $\delta^{15}N_{NSOs}$ and $\delta^{15}N_{Asp}$ in oils from the Tarim Basin are determined. The conversion and fractionation of N isotopes between distinct nitrogenous components were discussed. In addition, combining with carbon isotope ($\delta^{13}C$) and biomarkers, this study clarified the influence of biomass compositions and redox conditions on the $\delta^{15}N$ values of different nitrogenous components, and reconstructed the marine N cycle during the early Paleozoic in the Tarim Basin.

2. Geological setting

The Tarim Basin, situated between the Paleo–Asian and Tethyan tectonic domains, is an inland superimposed basin with an area of 5.6×10^5 km^2 that has undergone multiple major stages in structural evolution (Zhu et al., 2019b; Ning et al., 2022). It is developed on the pre-Sinian crystalline basement in the northwest of China, and can be divided into five uplifts and six depressions (Fig. 1) (Shi et al., 2017). The Paleozoic marine deposits and Meso–Cenozoic continental clastic deposits are widely developed in this basin (Hu et al., 2016; Zhu et al., 2019a,b). The Paleozoic marine strata, including the Lower Cambrian, Middle–Upper Cambrian, and Middle–Upper Ordovician source rocks, are the vital marine source rocks that produce massive oils in China (Li et al., 2020). Exploration in recent decades shows that these source rocks are distributed heterogeneously in different areas of the Tarim Basin (Fig. 2) (Liu et al., 2017). The Lower Cambrian source rocks are mostly located in the north of Bachu uplift, the east of Manjiaer Depression, the Tazhong uplift, and the south of Awati Depression. The Middle–Upper Cambrian source rocks are largely situated in the Tadong Uplift. The Middle–Upper Ordovician source rocks are located in the western Manjiaer Depression (Zhang et al., 2012; Liu et al., 2017). Due to the abundant source rocks and complex tectonic evolution, this basin is featured by multiple resources, multiple reservoirs, and multi-stage accumulation (Zhu et al., 2019a,b).

The Bashituo (BST) area is situated in the northwest of Markit slope. This region is a structural anticline with EW strike, and is mainly controlled by the BST fault, which is an NNE-dipping thrust fault of nearly EW-trending and north-to-south nappe (Cui et al., 2013; Guo et al., 2021). The BST structure basically maintained the topographical features of west-high and east-low in the pre-Permian, and was slowly uplifted after the Indosinian (Song et al., 2019; Zhu et al., 2019a,b). During the Late Himalayan, the anticline turned into a trend of east-high and west-low (Zhu et al., 2019b). The BST oil field is one of the earliest discovered oil fields in the Southwest Depression, and the oils are mainly reserved in the Devonian and Carboniferous strata (Cui et al., 2013). The distribution of these oils is strictly controlled by the BST fault (Song et al., 2019; Guo et al., 2021).

The Halahatang (HLHT) Sag, a secondary tectonic unit located in the south of Tabei Uplift covering an approximate area of 4000 km^2, is a favorable region for hydrocarbon accumulation (Cheng et al., 2013; Ning et al., 2022). This sag develops Proterozoic–Devonian marine sediments, Carboniferous–Permian marine-terrigenous sediments, and Triassic–Quaternary terrestrial sediments (Zhu et al., 2019a; Liu et al., 2022). Among them, the Ordovician marine strata are the main oil-bearing strata (Liu et al., 2022). This area experienced three stages of tectonic evolution, i.e., the large southern dip slope in the Late Caledonian period, the synclinal structure in the Early Hercynian period, and the present sag formed in the Yanshanian–Himalayan period (Chang et al., 2017). At

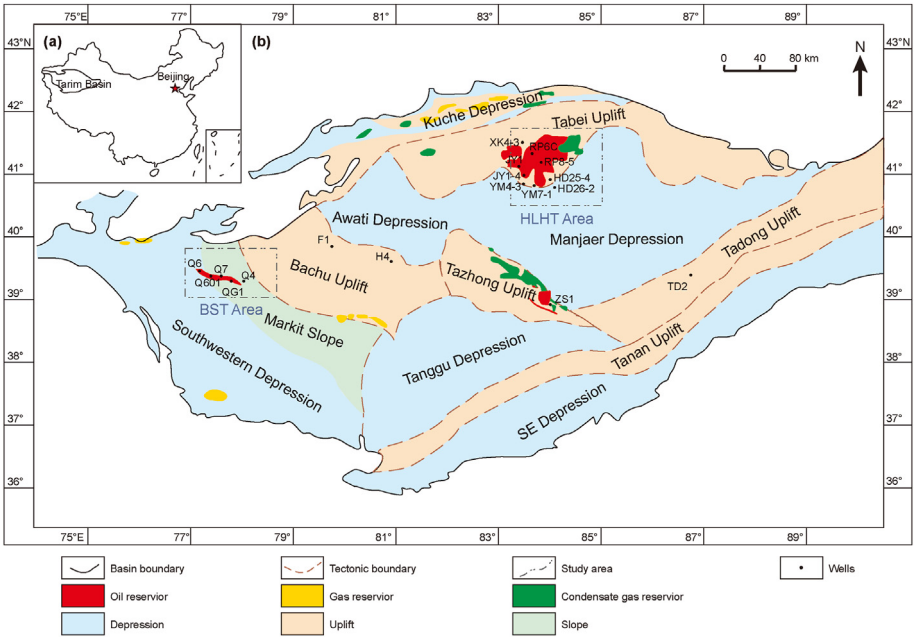

Fig. 1. Tectonic division and sample locations in the Tarim Basin (Zhang and Huang, 2005).

present, the HLHT Sag exhibits a large west-dipping nose-shaped structure (Zhu et al., 2019a).

3. Samples and experiments

3.1. Sample preparation

The thermal evolution of Paleozoic marine sediments in the Tarim Basin is relatively high, and light oil and condensate oil are mainly produced in most blocks (Cui et al., 2013; Tang et al., 2019). The N content of crude oil in these blocks is low, resulting in difficulties in the accurate determination of nitrogen isotopes. Therefore, in this study, the nitrogenous components were separated and enriched, and then the nitrogen isotope of each component was tested and analyzed. A total of 14 oils were analyzed in this paper, including 9 Ordovician crude oils from the HLHT area and 5 Devonian–Carboniferous crude oils from the BST area.

This study innovatively adopted a method that could separate crude oil samples weighing up to 2 g in a single operation (conventional method can only separate 20–30 mg) to ensure sufficient nitrogen content for the detection of nitrogen isotopes. To increase the recovery efficiency of N, the samples were first de-asphalted using *n*-heptane by 1 h heating at 50 °C for intensive dissolution. Saturate (Sat), aromatic (Aro), and NSOs fractions were separated using a 1-meter chromatographic column (alumina) via sequential elution with *n*-heptane, toluene, and toluene/ethanol (1:1). This method can retain the N in Aro to NSOs to avoid nitrogen loss.

3.2. Isotopic analysis

All isotopic analyses were carried out at the National Key Laboratory of Petroleum Resources and Engineering. Nitrogen and carbon isotope were determined by an Isoprime precisION mass spectrometer coupled to a vario ISOTOPE cube elemental analyzer. In the experiment, the helium was served as carrier gas and high-purity oxygen was used as the combustion gas (pressure: 1200–1250 mbar, flow rate: 20 mL/min). The temperature of oxidation tube in the reaction furnace was 1080 °C, and that of the reduction tube was 850 °C. The $\delta^{15}N$ values were documented relative to atmospheric N_2 and were calibrated by three standard materials, i.e., USGS25 ($\delta^{15}N$: −30.4‰, standard deviation (SD): 0.4‰), caffeine ($\delta^{15}N$: 1.0‰, SD: 0.2‰) and GSUS-62 ($\delta^{15}N$: 20.17‰, SD: 0.2‰). The $\delta^{13}C$ values were calibrated to the Vienna Pee Dee Belemnite (VPDB) standard and were calculated by two standard reference materials, i.e., USGS-24 ($\delta^{13}C$: 14.0‰, SD: 0.2‰) and, Oil-Lab ($\delta^{13}C$: −30.1‰, SD: 0.2‰). Typical reproducibility of analyses was 0.5‰ for $\delta^{15}N$ and 0.2‰ for $\delta^{13}C$.

3.3. Gas chromatography-mass spectrometry

Saturated and aromatic fractions were detected by gas chromatography-mass spectrometry (GC–MS) to obtain the composition of molecular biomarkers at the aforementioned laboratory. GC analysis was undertaken with an Agilent 6890 gas chromatograph and an Agilent Model 5975i mass selective detector, which equipped with an HP-5 MS fused silica capillary column, using helium as the carrier gas. The MS source was worked in the mode of electron impact with 50–600 Da scanning range and 70 eV ionization energy. The heating procedure was as follows: for saturated hydrocarbons, the initial temperature of the GC oven was 50 °C and held for 1 min, then heated to 120 °C with a rate of 20 °C/min, finally to 310 °C at a rate of 3 °C/min and held for 25 min; for aromatic hydrocarbons, the original temperature of the oven was also 50 °C and held for 1 min, and then programmatically heated to 310 °C with a rate of 3 °C/min and held for 16 min.

4. Results

4.1. Nitrogen isotopic compositions

The $\delta^{15}N$ values of the oils from BST and HLHT areas are shown in Table 1. The $\delta^{15}N_{NSOs}$ values of HLHT oils were in the range of 1.8‰–3.8‰ (av. = 2.7‰), and their $\delta^{15}N_{Asp}$ values varied from 4.8‰ to 9.6‰ (av. = 6.6‰) (Table 1 and Fig. 3). The offsets between $\delta^{15}N_{Asp}$ and $\delta^{15}N_{NSOs}$ (i.e., $\delta^{15}N_{Asp}$-$\delta^{15}N_{NSOs}$) ranged from 3.2‰ to 6.9‰ (av. = 4.4‰), indicating the heavier $\delta^{15}N$ values of asphaltenes

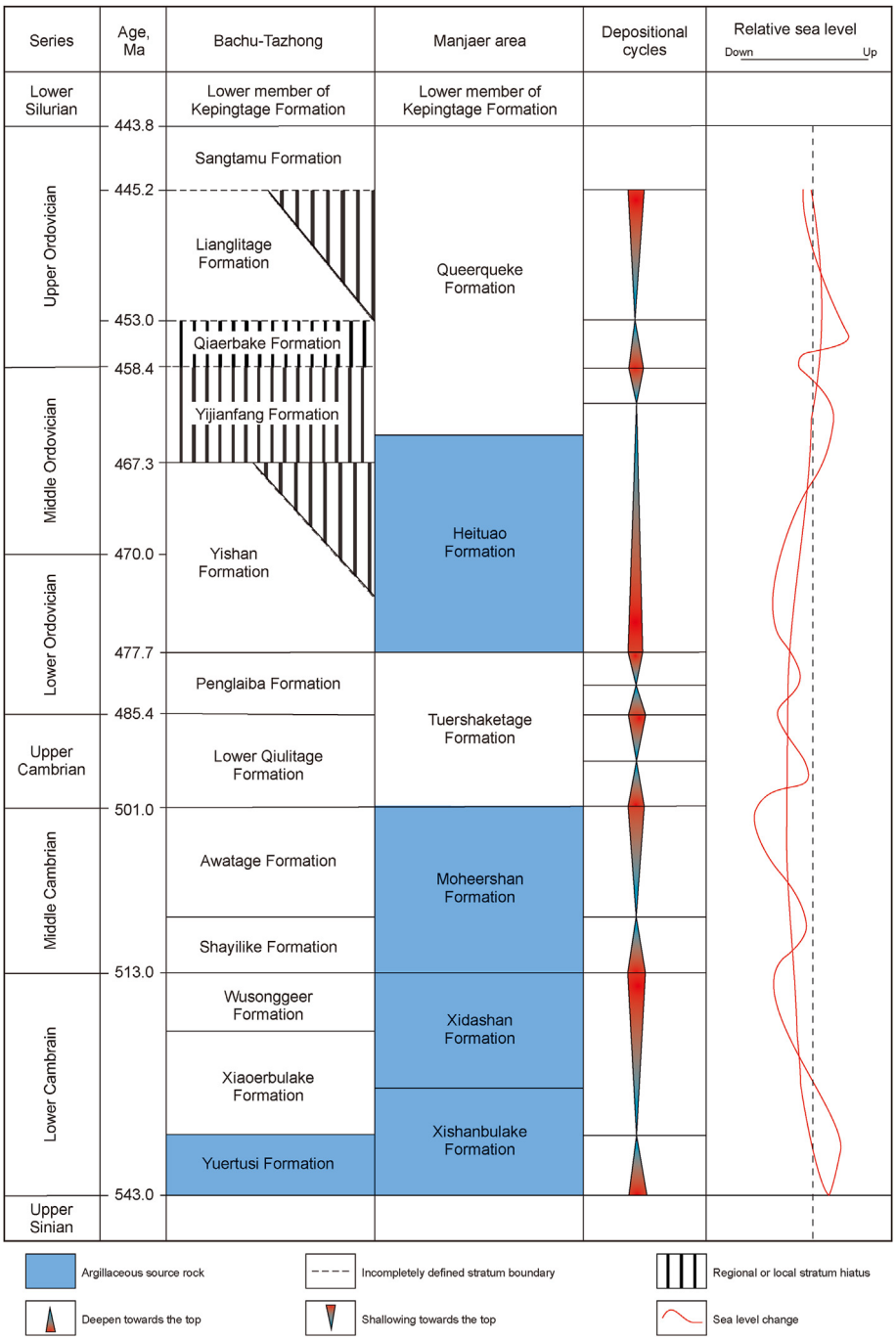

Fig. 2. Distribution of Paleozoic strata and conventional source rocks in the Tarim Basin (Liu et al., 2017).

than those of NSOs (Table 1 and Fig. 3).

The $\delta^{15}N_{NSOs}$ and $\delta^{15}N_{Asp}$ values of BST oils varied over the range of 5.7‰–8.5‰ (av. = 6.8‰) and 9.6‰–10.9‰ (av. = 10.4‰), respectively (Table 1 and Fig. 3). The values of $\delta^{15}N_{Asp}$-$\delta^{15}N_{NSOs}$ were 2.2‰–3.5‰ (av. = 2.7‰), similar to the tendency of heavier $\delta^{15}N_{Asp}$ values than $\delta^{15}N_{NSOs}$ in HLHT oils (Table 1 and Fig. 3).

4.2. Carbon isotopic compositions

The $\delta^{13}C$ values in whole oils and their fractions from the BST and HLHT areas are presented in Table 1. In the HLHT area, the $\delta^{13}C$ values of oils ranged from −32.8‰ to −32.3‰ (with an average of −32.5‰) (Table 1 and Fig. 4). In the BST area, the $\delta^{13}C$ values of oils were slightly lighter than those in HLHT oils, ranging from −34.1‰ to −34.8‰ (with an average of −34.5‰) (Table 1 and Fig. 4). The $\delta^{13}C$ values in whole oils and their fractions of the BST area followed the normal law of $\delta^{13}C_{Sat} < \delta^{13}C_{Oil} < \delta^{13}C_{Aro} < \delta^{13}C_{NSOs} < \delta^{13}C_{Asp}$, whereas the HLHT oils had an abnormal law of $\delta^{13}C_{Sat} < \delta^{13}C_{Oil} < \delta^{13}C_{Aro} < \delta^{13}C_{NSOs} > \delta^{13}C_{Asp}$ (Table 1 and Fig. 4). The $\delta^{13}C_{Asp}$ values in HLHT oils were clearly lighter than those of $\delta^{13}C_{NSOs}$, and were equal to or even lighter than those of aromatic hydrocarbons (Table 1 and Fig. 4).

Table 1
Isotopic data for fractions of BST and HLHT oils.

Area	Well	Depth, m	$\delta^{13}C_{Oil}$, ‰	$\delta^{13}C_{Sat}$, ‰	$\delta^{13}C_{Aro}$, ‰	$\delta^{13}C_{NSOs}$, ‰	$\delta^{13}C_{Asp}$, ‰	$\delta^{15}N_{NSOs}$ ‰	$\delta^{15}N_{Asp}$, ‰	$\delta^{15}N_{Asp}$-$\delta^{15}N_{NSOs}$, ‰
HLHT	HD25-4	6721.0–6820.0	−32.3	−33.5	−32.0	−31.1	−31.9	2.4	5.6	3.2
	HD26-2	6548.4–6653.0	−32.5	−33.4	−31.9	−31.1	−32.0	1.8	5.3	3.5
	JY1	7154.6–7208.4	−32.4	−32.8	−31.3	−29.7	−31.0	3.5	8.4	4.9
	JY1-4	7123.5–7224.0	−32.4	−33.1	−32.2	−31.6	−32.2	2.0	6.2	4.2
	RP6C	5746.7	−32.5	−32.7	−31.4	−29.6	−31.7	1.8	5.0	3.2
	RP8-5	6857.0–6900.0	−32.8	−33.0	−32.2	−31.8	−32.9	2.0	6.8	4.8
	XK4-3	6753.39–6837.0	−32.8	−32.8	−32.6	−32.0	−32.8	2.7	7.3	4.6
	YM5-3	7222.0–7292.0	−32.7	−33.0	−31.4	−30.5	−31.5	2.5	9.4	6.9
	YM7-1	7243.0–7334.0	−32.5	−32.9	−31.9	−31.1	−32.8	2.8	7.2	4.4
BST	Q4	4857.0–4890.0	−34.6	−35.6	−34.3	−34.0	−33.5	8.5	10.8	2.3
	Q7	5065.0–5075.0	−34.4	−34.9	−34.1	−34.0	−31.1	7.5	9.6	2.1
	QG1	4861.0–4864.5	−34.4	−35.1	−34.6	−34.7	−33.1	7.1	10.1	3.0
	Q601	5397.8–5470.2	−34.1	−34.7	−33.6	−33.5	−32.7	7.3	9.6	2.3
	Q6	6721.0–6820.0	−34.8	−34.7	−33.5	−33.3	−32.6	6.9	10.4	3.5

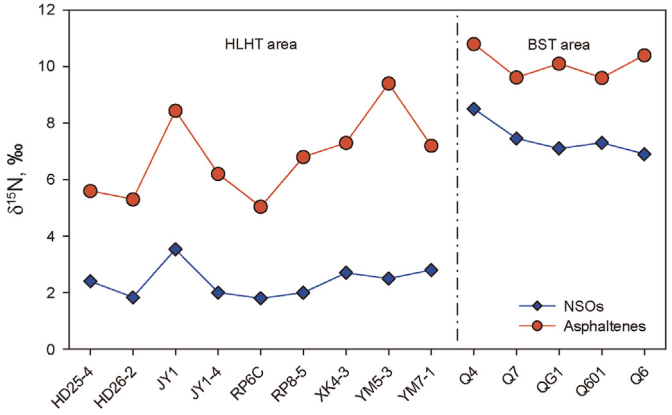

Fig. 3. The distribution of $\delta^{15}N_{Asp}$ and $\delta^{15}N_{NSOs}$ in the studied oils.

4.3. Organic geochemistry

The selected biomarker parameters are exhibited in Table 2. The pristine/phytane (Pr/Ph) ratios of the studied oils were in the range of 0.80–1.39. The pristine/*n*-C_{17} (Pr/*n*-C_{17}) values of the crude oils in BST and HLHT areas were generally <0.5 (0.19–0.24 and 0.32–0.42, respectively), and the phytane/*n*-C_{18} (Ph/*n*-C_{18}) values were generally <0.6 (0.14–0.17 and 0.40–0.55, respectively) (Table 2). C_{22}/C_{21} tricyclic terpane (C_{22}TT/C_{21}TT), C_{21} tricyclic terpane/C_{23} tricyclic terpane (C_{21}TT/C_{23}TT), C_{28}/C_{29} sterane ratios and C_{27}/C_{28}20R triaromatic sterane (TAS) ratios of BST oils were <0.35 (0.27–0.34), >0.7 (0.77–0.89), >0.7 (0.73–0.85), and >0.4 (0.44–0.75), respectively (Table 2). These ratios for HLHT oils were >0.35 (0.35–0.53), <0.7 (0.41–0.67), <0.5 (0.14–0.43), and <0.4 (0.15–0.33), respectively (Table 2). The gammacerane to C_{31}22R homohopane (Ga/C_{31}R) ratios in the BST and HLHT oils ranged from 0.55 to 1.02 and from 0.20 to 0.49, respectively (Table 2).

5. Discussion

5.1. Relationship between the $\delta^{15}N_{NSOs}$ and $\delta^{15}N_{asp}$

The $\delta^{15}N_{asp}$ values were heavier than $\delta^{15}N_{NSOs}$ values in BST and HLHT oils (Table 1 and Fig. 3). These results implied that the $\delta^{15}N_{NSOs}$ and $\delta^{15}N_{Asp}$ values might be genetically related. Asphaltenes, the intermediate products in the process of kerogen transforming into free hydrocarbon, are copolymers composed of aromatic rings connected by aliphatic and/or cycloalkane chains (Bandurski, 1982; Wu et al., 2020). During the thermal evolution, complex variations occurred in asphaltenes, such as decarboxylation, dehydroxylation, deamination, demethylation, and C–C bond breaking (Pereira et al., 2019). In this process, asphaltenes were converted into saturated hydrocarbons, aromatic hydrocarbons, and NSOs, accompanied by the transfer of N. In addition, the artificially simulated experiments conducted on NSOs showed that as the heating temperature increased, the main chemical reaction of NSOs was secondary cracking into hydrocarbons, rather than polycondensation into higher-molecular-weight asphaltenes (Behar et al., 2008; Prado et al., 2017). This indicated potential directional N transfer from asphaltenes to NSOs.

According to the kinetic isotopic effect, the required activation energy of reactions with isotopically light species (i.e. ^{14}N) is significantly lower than that of reactions with isotopically heavy species (i.e. ^{15}N), and the reaction rate of the former is usually faster

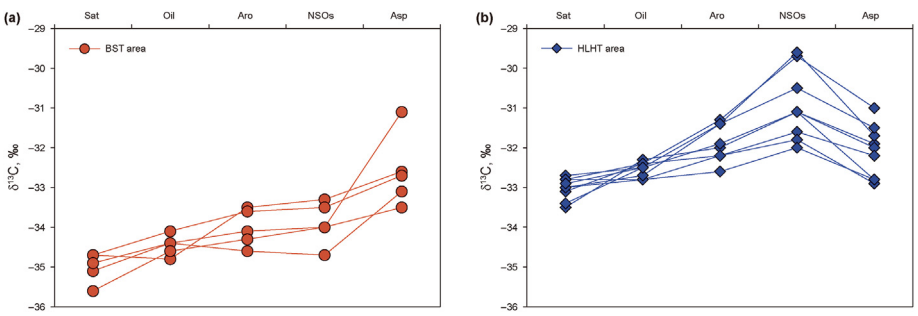

Fig. 4. Carbon isotope distribution of oils and their fractions in **(a)** BST area and **(b)** HLHT area.

Table 2
Selected biomarker parameters related to acyclic isoprenoids, tricyclic terpanes, steranes and triaromatic steroids.

Area	Well	Depth, m	Pr/Ph	Pr/nC_{17}	Ph/nC_{18}	$C_{21}TT/C_{23}TT$	$C_{22}TT/C_{21}TT$	C_{28}/C_{29} sterane	C_{27}/C_{28} TAS (20R)	Ga/$C_{31}R$
HLHT	HD25-4	6721.0–6820.0	0.83	0.42	0.55	0.41	0.44	0.20	0.25	0.36
	HD26-2	6548.4–6653.0	0.80	0.39	0.52	0.41	0.53	0.24	/	0.49
	JY1	7154.6–7208.4	0.80	0.32	0.43	0.60	0.37	0.38	0.33	0.48
	JY1-4	7123.5–7224.0	0.85	0.34	0.44	0.54	0.38	0.32	0.15	0.36
	RP6C	5746.7	0.83	0.33	0.40	0.54	0.39	0.13	0.24	0.43
	RP8-5	6857.0–6900.0	0.86	0.35	0.46	0.52	0.40	0.18	0.23	0.34
	XK4-3	6753.39–6837.0	0.86	0.41	0.49	0.49	0.38	0.15	/	0.33
	YM5-3	7222.0–7292.0	0.84	0.32	0.44	0.67	0.35	0.43	/	0.20
	YM7-1	7243.0–7334.0	0.88	0.36	0.44	0.54	0.36	0.15	/	0.31
BST	Q4	4857.0–4890.0	1.34	0.22	0.14	0.77	0.28	0.78	0.75	1.02
	Q7	5065.0–5075.0	1.34	0.19	0.15	0.83	0.28	0.85	/	0.82
	QG1	4861.0–4864.5	1.34	0.21	0.14	0.89	0.27	0.80	/	0.60
	Q601	5397.8–5470.2	1.25	0.24	0.17	0.81	0.27	0.73	0.44	0.72
	Q6	6721.0–6820.0	1.39	0.19	0.15	0.80	0.34	0.84	/	0.55

Notes: / not determined.

than the latter (Galimov, 2006). Therefore, in the cracking process of asphaltenes, ^{14}N tended to be enriched in NSOs with relatively small molecular structures or non-hydrocarbon gases, whereas the retained ^{15}N was more inclined to accumulate in residual asphaltenes with a higher degree of aromatic ring polymerization. This demonstrated that the relationship of $\delta^{15}N_{Asp}>\delta^{15}N_{NSOs}$ was the result of N transfer and associated kinetic isotope fractionation during the thermal evolution of OM.

5.2. Nitrogen isotope and biomass composition

5.2.1. Biomass composition

Common geochemical indicators reflecting the differences in OM of marine source rocks and crude oils from the Tarim Basin include Pr/n-C_{17}, Ph/n-C_{18}, $C_{22}TT/C_{21}TT$, $C_{21}TT/C_{23}TT$, C_{28}/C_{29} sterane, C_{27}/C_{28}TAS (20R), and triaromatic dinosteroids. The Pr/n-C_{17} vs. Ph/n-C_{18} plot showed that the bio-precursors in all studied oils were algae, and the thermal maturity of BST oils was higher than that of HLHT oils (Fig. 5) (Shanmugam, 1985). The high content of tricyclic terpanes also indicated the contribution of algae (Xiao et al., 2019). The C_{23} member is the predominant homologue of marine oils, whereas the C_{19} and C_{20} members are more enriched in terrestrial oils (Zhang and Huang, 2005; Tao et al., 2015). As exhibited in Fig. 6(a)–(b), the relatively high abundance of the $C_{23}TT$ in all oils implied the high contribution of marine OM. The BST oils featured high $C_{24}/C_{23}TT$ (>0.7) and low $C_{22}/C_{21}TT$ (<0.3), while the HLHT oils featured low $C_{24}/C_{23}TT$ (<0.7) and high $C_{22}/C_{21}TT$ (>0.3) (Table 2). The distribution patterns of $C_{19}TT$ to $C_{24}TT$ in BST and HLHT oils were also different (Fig. 6(a)–(b)). These results revealed two oil families in the studied areas.

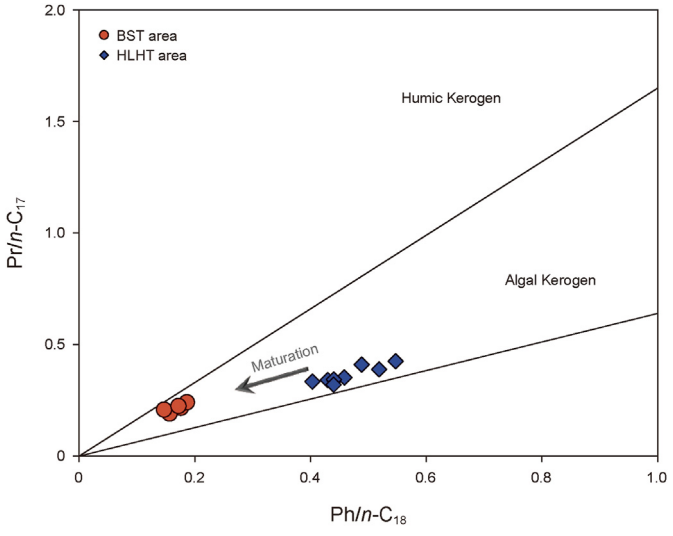

Fig. 5. Cross plots of Pr/n-C_{17} vs. Ph/n-C_{18} alkane ratios of the studied oils from the Tarim Basin (Zhang and Huang, 2005).

The relative abundance of C_{27-29} regular steranes can be used to broadly infer the contributions of various types of algae (Volkman, 2003; Xia et al., 2022). Grantham and Wakefield (1988) reported that the increase in C_{28} regular sterane was resulted from the evolution of phytoplankton (e.g., dinoflagellates) (Grantham and Wakefield, 1988; Li et al., 2012). The C_{28}/C_{29} regular sterane ratios in BST oils (>0.73) were higher than those in HLHT oils (<0.43) (Table 2), and the C_{28} regular sterane content in HLHT oils was clearly low (Fig. 6(c)–(d)). Thus, the contributions of these specific phytoplankton assemblages to HLHT oils may be less than those to BST oils. TAS may be generated by aromatization and removal of a methyl group ($-CH_3$) from monoaromatic steroids, and they potentially hold genetic information about oils and corresponding source rocks, similar to C_{27-29} regular steranes (Li et al., 2012). The HLHT oils were featured by higher C_{28} 20R TAS and C_{28} 20S TAS, compared to their corresponding homologues, than BST oils (Fig. 6(e)–(f)). In addition, triaromatic dinosteroid is regarded as the almost exclusive compound, prevalently presenting in natural product of dinoflagellates (Li et al., 2012). The contents of triaromatic dinosteroids in BST oils were high, whereas they could not be detected in HLHT oils (Fig. 6(g)–(h)). The above characteristics imply that the two oil families were derived from different types of algae.

The above geochemical indicators provide sufficient evidence for oil-source correlations (Zhang and Huang, 2005; Li et al., 2012; Bao et al., 2018). According to the geochemical characteristics of Cambrian–Ordovician source rocks, and the associated oils documented by previous studies, the BST oils were considered to be generated from the Lower Cambrian source rocks, and the HLHT oils originated from the Middle–Upper Ordovician source rocks (Hu et al., 2016; Bao et al., 2018; Huo et al., 2019; Li et al., 2020). It has been proven that algae are the preponderant bioprecursors of OM in the Early Paleozoic of Tarim Basin (Zhu et al., 2016; Tang et al., 2019), and have identified various types (including planktonic and benthic algae) in source rocks with different carbon isotope characteristics (Chen et al., 2015; Hu et al., 2019). The study reported by Hu et al. (2014) for the sedimentary OM in the Tarim Basin indicated that the $\delta^{13}C$ values of kerogen dominated by benthic algae ($\delta^{13}C_{kerogen} < -34.0‰$) were lower than those of

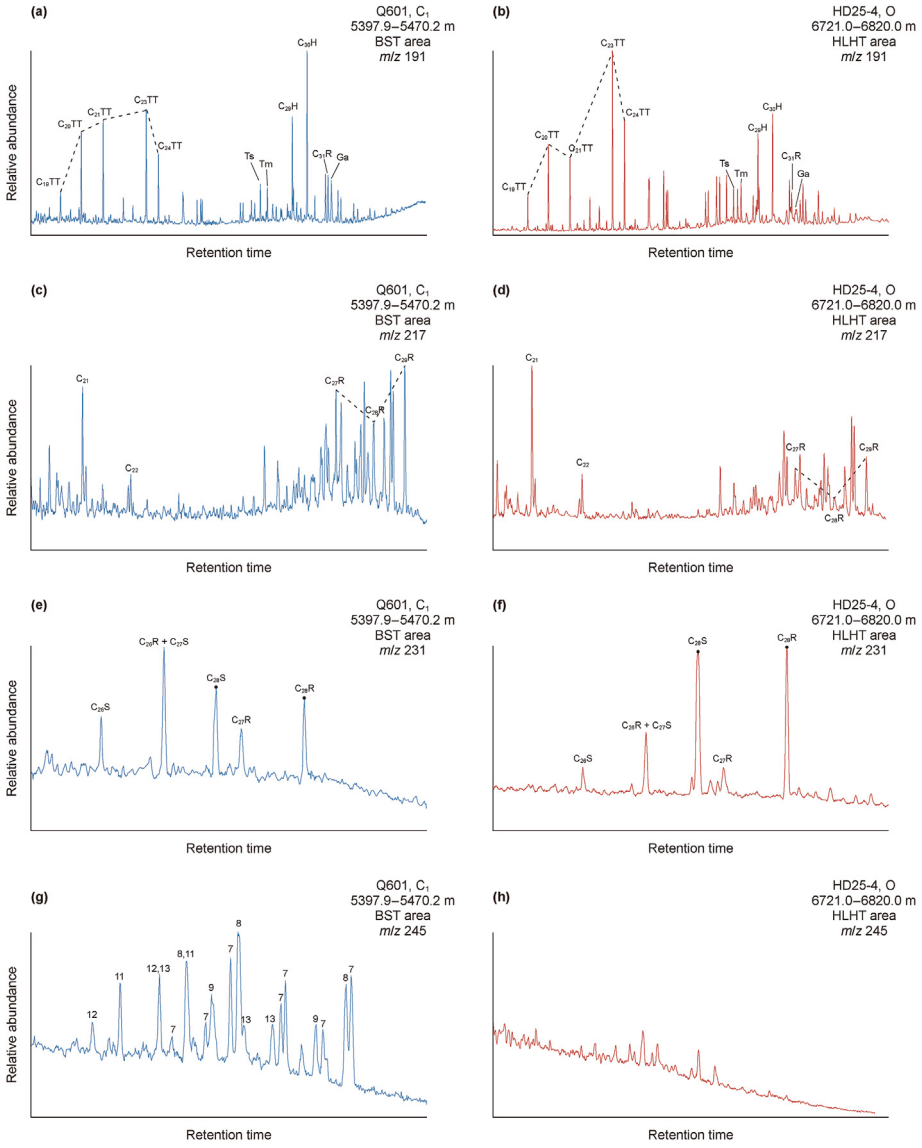

Fig. 6. Mass chromatograms (*m/z* 191; *m/z* 217; *m/z* 231; *m/z* 245) in crude oils from the BST **(a, c, e, g)** and HLHT **(b, d, f, h)** areas, showing the distribution of tricyclic terpane, regular sterane, triaromatic steranes, and methyl triaromatic steroids, respectively. In **(g)**, peak 7 represents 4,23,24- trimethyltriaromatic dinosteranes (C_{29} triaromatic dinosteranes), peak 8 represents 4-methyl-24-ethyltriaromatic steroids (C_{29} triaromatic steroids), peak 9 represents 3-methyl-24-ethyltriaromatic steroids (C_{29} triaromatic steroids), peak 11 represents 4-methyltriaromatic steroids (C_{27} triaromatic steroids), peak 12 represents 3-methyltriaromatic steroids (C_{27} triaromatic steroids), peak 13 represents 3,24-dimethyltriaromatic steroids (C_{28} triaromatic steroids).

kerogen dominated by planktonic algae ($\delta^{13}C_{kerogen} > -30.0‰$). Their different $\delta^{13}C$ values were resulted from the differences in carbon sources and photosynthetic fractionation (Chen et al., 2015; Liu et al., 2017). In this study, the $\delta^{13}C$ values of BST oils were relatively lower than those of HLHT oils, with the range of −35.0‰ to −34.0‰ and −33.0‰ to −32.0‰, respectively. According to the carbon isotope fractionation of conversion from kerogen to oil ($\delta^{13}C$ varies in the range of 2‰–3‰) (Tissot and Welte, 1984), the BST oils originated from benthic and planktonic algae, while the contribution of benthic algae to HLHT oils was much less. Moreover, based on maceral identification, Hu et al. (2019) found that benthic algae (e.g., macro Rhodophyta) were the main components in the Lower Cambrian source rocks, and the Middle–Upper Ordovician source rocks were dominated by planktonic algae (e.g., Cyanobacteria). The algal characteristics revealed by geochemical indicators of oils were in agreement with the microscopic characteristics of the related source rocks.

5.2.2. Response of nitrogen isotopes in different fractions to biomass composition

The study conducted on modern algae showed that the $\delta^{15}N$ values of planktonic algae (3.4‰–7.2‰) were generally lower than those of benthic algae (5.2‰–9.7‰), which was mainly caused by the different N sources (Miyake and Wada, 1967). Planktonic algae live in the surface water, and atmospheric N_2 and inorganic N ions are their main N sources. The $\delta^{15}N$ values of atmospheric N_2 is close to 0‰ (Miyake and Wada, 1967). On the surface of seawater, N_2 gas is converted into NH_4^+ by N-fixing bacteria (mainly cyanobacteria) with a slight N-isotope fractionation effect (fractionation factor: α~0.994–1.0024), and the oxidation of NH_4^+ by aerobic bacteria is also accompanied by a comparatively small isotopic fractionation factor (α~1.02), resulting in the enrichment of ^{14}N in planktonic algae (Delwiche and Steyn, 1970; Chen et al., 2019). Benthic algae take roots in the muddy substrates and mainly absorb ammonium N and DON (including the dissolved N from planktonic debris,

directly deposited N, and N retained by benthic debris), resulting in the enrichment of ^{15}N. In this study, BST oils were mainly derived from benthic algae and enriched in ^{15}N, while the HLHT oils mainly originated from planktonic algae with light $\delta^{15}N$ values. However, due to both influence of bioprecursors and redox conditions on $\delta^{15}N$, it is still uncertain whether the differences in $\delta^{15}N$ of oils from the two regions are the result of inheriting differences in OM and being strengthened by environmental factors, or the manifestation that the biological characteristics have been completely overprinted by redox conditions. Thus, the response of $\delta^{15}N$ to different factors need to be further confirmed by other parameters.

Although the intrinsic link between the biomarker parameters and algae categories was not clear, the biomarker had identified the differences in OM of the BST and HLHT oils as discussed above. In this study, correlations between $\delta^{15}N$ values of different nitrogenous fractions and biomarkers parameters (including $C_{22}TT/C_{21}TT$, $C_{21}TT/C_{23}TT$, Pr/*n*-C_{17} and C_{28}/C_{29} regular sterane) displayed that the $\delta^{15}N_{Asp}$ values had more obvious correlations with these biomarker parameters than the $\delta^{15}N_{NSOs}$ values (Figs. 7 and 8). The ratios of $C_{21}TT/C_{23}TT$ and C_{28}/C_{29} regular sterane increased with the increase of $\delta^{15}N_{Asp}$ values, whereas the $C_{22}TT/C_{21}TT$ and Pr/*n*-C_{17} values exhibited the opposite pattern, indicating a close connection between $\delta^{15}N_{Asp}$ and biological characteristics. Based on the above discussion that BST oils were mainly contributed by benthic algae (with heavy $\delta^{15}N$), it was speculated that the heavy $\delta^{15}N_{Asp}$ values and the increase of $C_{21}TT/C_{23}TT$ and C_{28}/C_{29} regular sterane ratios are related to the increasing proportion of benthic algae in BST oils (Fig. 7). The distribution of $\delta^{15}N_{NSOs}$ values was relatively concentrated within the region of BST and HLHT areas, and supported the view that dividing all oils into two families, but the correlations with biomarkers were not as significant as the $\delta^{15}N_{Asp}$ values (Fig. 8). Therefore, the difference in $\delta^{15}N_{Asp}$ values may point towards the inheritance of biological characteristics influences that has not been comprehensively covered by the influence of redox conditions, while the inheritance of bioprecursors in $\delta^{15}N_{NSOs}$ values seems to have been overprinted by other factors as discussed in section 5.3.2.

Sweeney and Kaplan (1980) suggested that the deposition of OM resulted in the accumulation of refractory fraction (kerogen), and the $\delta^{15}N$ values of kerogen were almost constant with those of the organisms (Sweeney and Kaplan, 1980; Waples and Sloan, 1980). In the process of oil generation from kerogen, asphaltenes is mainly produced by the thermal degradation of biological macromolecules and contains most of the N atoms. Previous studies conducted on the pyrolysis of the asphaltenes demonstrated that only 1% N was removed during the heating treatment, whereas more sulfur (23%) and most of the oxygen (81%) were lost due to this treatment (Bandurski, 1982; Rashid et al., 2019). These results show that the N in OM can be well preserved in asphaltenes during the thermal evolution. That is the possible reason why the $\delta^{15}N_{Asp}$ values are more likely to record the primitive $\delta^{15}N$ of OM.

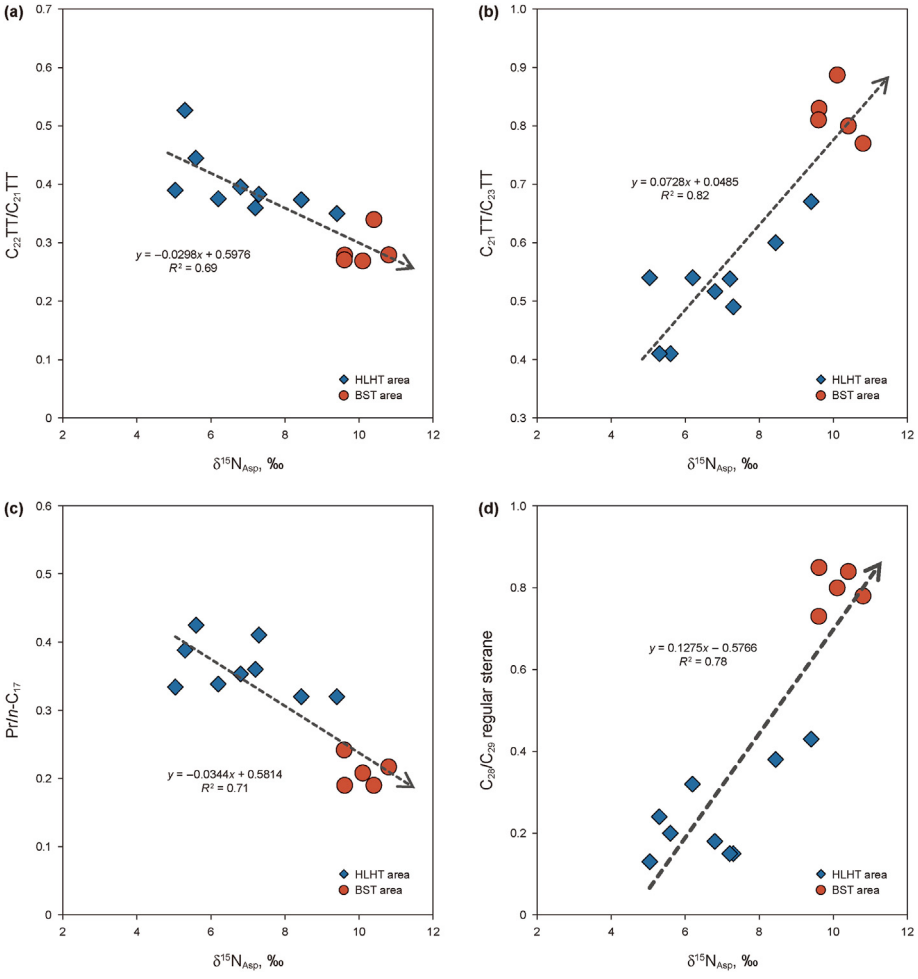

Fig. 7. Relationships between biomarkers and $\delta^{15}N_{Asp}$. **(a)** $C_{22}TT/C_{21}TT$ vs. $\delta^{15}N_{Asp}$, **(b)** $C_{21}TT/C_{23}TT$ vs. $\delta^{15}N_{Asp}$, **(c)** Pr/*n*-C_{17} vs. $\delta^{15}N_{Asp}$, **(d)** C_{28}/C_{29} regular sterane vs. $\delta^{15}N_{Asp}$.

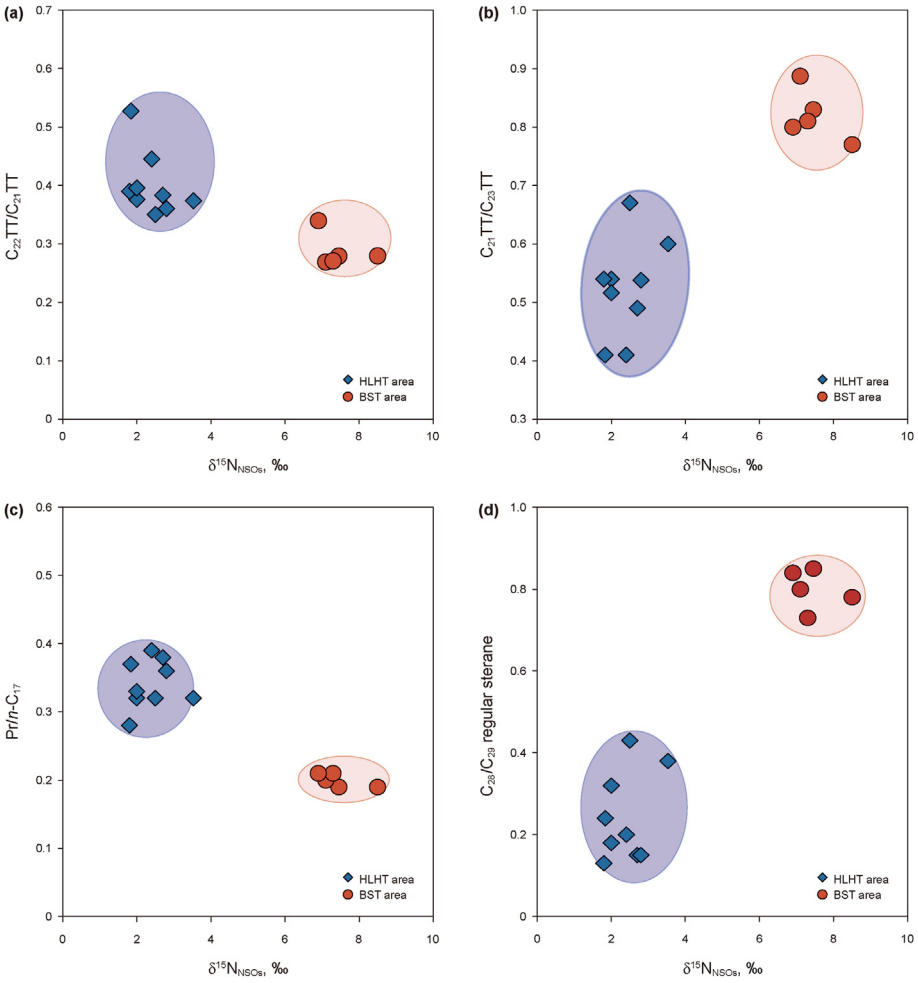

Fig. 8. Relationships between biomarkers and $\delta^{15}N_{NSOs}$. **(a)** $C_{22}TT/C_{21}TT$ vs. $\delta^{15}N_{NSOs}$, **(b)** $C_{21}TT/C_{23}TT$ vs. $\delta^{15}N_{NSOs}$, **(c)** Pr/*n*-C_{17} vs. $\delta^{15}N_{NSOs}$, **(d)** C_{28}/C_{29} regular sterane vs. $\delta^{15}N_{NSOs}$.

5.3. Nitrogen isotope and redox conditions

5.3.1. Redox conditions of the water column

Pr/Ph is a common biomarker parameter used to reconstruct paleo-redox conditions. In this study, the Pr/Ph ratios of BST oils ranged from 1.25 to 1.39, and those of the HLHT oils were in the range of 0.80–0.88, which suggested dysoxic and dysoxic–anoxic conditions, respectively. However, previous studies had revealed that the BST oils were formed under a stronger anoxic environment than HLHT oils (Hu et al., 2016; Song et al., 2019). Powell (1988) reported that the Pr/Ph ratios would be affected by other factors (e.g. maturity) when it was in the range of 0.80–2.50, and it could not be directly used to reveal redox conditions. With the increase in oil maturity, the Pr/Ph ratios generally increase, and the ratios of Ph/*n*-C_{18} decrease (Ten Haven et al., 1987). As displayed in Fig. 5, the ratios of Ph/*n*-C_{18} in BST oils are clearly lower than those in HLHT oils, indicating the higher maturity of BST oils than those of HLHT oils. Accordingly, the higher Pr/Ph ratios of BST oils may be caused by higher thermal maturity, resulting in inaccuracies of Pr/Ph ratios for the indication of redox conditions in this study.

Gammacerane (Ga) indicates a stratified water column in marine source-rock depositional environments, which commonly results from hyper salinity at depth (Sinninghe Damste et al., 1995). Gammacerane index is used to reveal the relative abundance of Ga, and is commonly expressed as Ga/$C_{30}\alpha\beta$ hopane (Ga/C_{30}H), 10 × Ga/(Ga + $C_{30}\alpha\beta$ hopane), and Ga/C_{31}22R homohopane (Ga/C_{31}R) (Peters et al., 2005). These parameters have a good response to the characteristics of depositional environment, i.e., the higher index indicates the higher salinity of water column, more obvious stratification, and more anoxic conditions (Xia et al., 2022; Ni et al., 2024). In this study, the relative abundance of $C_{30}\alpha\beta$ hopane in the Cambrian and Ordovician oils in Tarim Basin is significantly affected by thermal maturity. Thus, compared to Ga/C_{30}H, Ga/C_{31}R is considered to be more suitable as an effective indicator to reflect the difference of sedimentary environment. According to the GC-MS results of all oils in this study, the Ga/C_{31}R ratios in BST oils (>0.5) were obviously higher than those of HLHT oils (<0.5), demonstrating that BST oils originated from the source rocks deposited in a more anoxic environment with high salinity and strong stratification, which is in agreement with previous studies for the Tarim Basin (Hu et al., 2016; Su et al., 2020).

During the deposition of Cambrian–Ordovician, the environment of global water column varies frequently and complicatedly (Su et al., 2020). In the Early Cambrian, the first large-scale transgression of the Phanerozoic occurred and the CO_2 content increased (Zhang et al., 2020). The first mass extinction event of the Phanerozoic occurred during this period, which represented the turning point of global biological evolution (Su et al., 2020). The deep hydrothermal activities brought a large amount of reducing gas, resulting in the rapid consumption of O_2 in bottom water and the acceleration of water column stratification (Zhang et al., 2020). The extremely anoxic condition in deep water provided good

conditions for the preservation of OM in sediments (Zhang et al., 2020). Furthermore, the carbon isotopic compositions of these sediments throughout the world were abnormally light during this period, which is similar to the characteristics of BST oils (<−34‰) (Hu et al., 2019; Shang et al., 2020). After the end of the first large-scale transgression, the sea level declined, the oxygen content increased, and the reducibility of water column decreased (Zhang et al., 2020). The second transgression occurred in the Middle–Late Ordovician, where the reducibility of water column was weaker than that in the Early Cambrian (Zhang et al., 2012; Chen et al., 2015).

Further evidence for depositional environment can be found in biomass compositions. Large planktonic algae are usually affected by wind and waves, and they accumulate in the nearshore zone (Mcnair and Chow-Fraser, 2003; Chen et al., 2015). They can be preserved in a standing water condition with shallow redox interface (Hu et al., 2014; Chen et al., 2015). The ultrananoplanktonic algae are small in size, have a slow sedimentation rate, and are difficult to be preserved, resulting in the lower contents of ultra-nanoplanktonic algae than those of large planktonic algae (Wu et al., 1999; Druzhkova, 2009). The distribution of benthic algae is mainly controlled by water depth, and most of them live in coastal zones (Wu et al., 1999; Druzhkova, 2009). Thus, the change of biomass composition can reveal variations in the transgression-regression sequence. The dominance of benthic algae in BST oils is due to better preservation under strong anoxic conditions, which resulted from the large-scale transgression during the Early Cambrian (Fig. 11(a)). An increase in the proportion of planktonic algae in HLHT oils indicates the relatively lower sea level and the shallower redox interface during the Middle–Upper Ordovician (Fig. 11(b)). In general, the original OM of BST oils are deposited in a stronger anoxic environment than those of HLHT oils.

5.3.2. Response of nitrogen isotopes in different fractions to redox conditions

To investigate the response of nitrogen isotopes in fractions to redox conditions, the correlations between $\delta^{15}N$ values (including $\delta^{15}N_{NSOs}$ and $\delta^{15}N_{Asp}$) and $Ga/C_{31}R$ were examined. As shown in Fig. 9, there is no significant correlation between $\delta^{15}N_{Asp}$ values and $Ga/C_{31}R$, whereas $\delta^{15}N_{NSOs}$ values and $Ga/C_{31}R$ had a strong non-linear relationship ($R^2 = 0.88$). These indicated that despite the influence of biological characteristics on $\delta^{15}N_{NSOs}$ values as mentioned above, $\delta^{15}N_{NSOs}$ values still exhibited a good response to paleoenvironmental variations in the water column. However, it

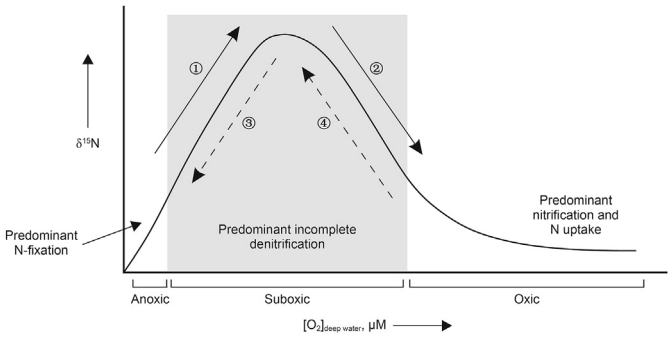

Fig. 10. Conceptual portrayal of the relationship between bulk sediment $\delta^{15}N$ values and deep water oxygen concentrations (Quan et al., 2008, 2013).

should be noted that the differences in $\delta^{15}N_{NSOs}$ caused by environmental variations are weakened by differences inherited from organisms in this study.

It is widely accepted that variations in water environment leads to differences in chemical reaction types and isotopic fractionation in the process of N cycle, which affects the $\delta^{15}N$ of source rocks and oils (Wang et al., 2018; Chen et al., 2019; Li et al., 2021; Wei et al., 2021; Yang et al., 2021). Quan et al. (2008) depicted a non-linear relationship model between the $\delta^{15}N$ values of sediments and oxygen concentrations of deep water (Fig. 10). It documents that the N cycle is predominated by N-fixation with a slight N-isotope effect (α~0.994–1.0024) under extremely anoxic conditions. Under fully oxic conditions, the $\delta^{15}N$ values reflect the isotopic fractionation due to nitrification (α~1.02) and N-fixation, while under suboxic conditions, the $\delta^{15}N$ values imply isotopic fractionation due to nitrification, denitrification and anammox (anaerobic ammonium oxidation). The comparatively higher isotopic fractionation factor in connection with anammox and denitrification (α~1.020–1.040) leads to higher $\delta^{15}N$ values in sediments (Quan et al., 2008; Chen et al., 2019). In this study, the BST oils originated from the source rocks deposited under obviously redox-stratified water column. The occurrence of a redox transition zone might promote denitrification and anammox, which caused the heavier $\delta^{15}N$ values of sediments and crude oils (Chen et al., 2023). In contrast, during the deposition of source rocks related to HLHT oils, the sea level was relatively low and the oxygen concentration of water column was high. The reproduction of planktonic algae decreased the vertical extent of the photic zone and the oxygen minimum zone, and

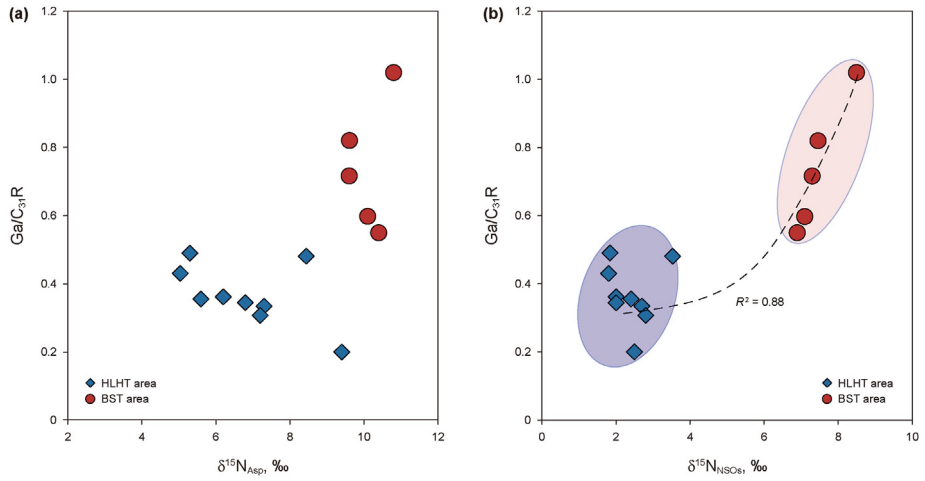

Fig. 9. Relationships of $Ga/C_{31}R$ with **(a)** $\delta^{15}N_{Asp}$, and **(b)** $\delta^{15}N_{NSOs}$.

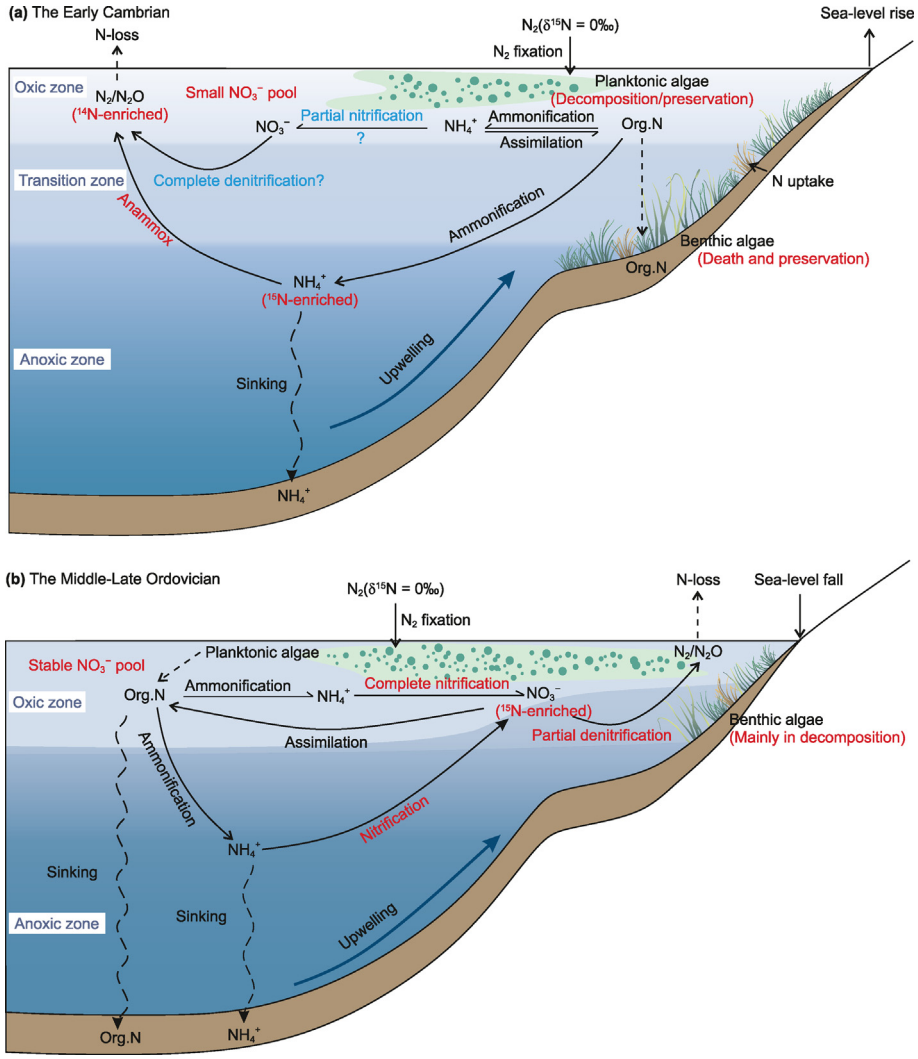

Fig. 11. Marine N cycle model during **(a)** the Early Cambrian and **(b)** the Middle–Late Ordovician in the Tarim Basin.

shallowed the redox interface. This would result in the limited reaction space of denitrification and anammox and relatively low $\delta^{15}N$ values.

5.4. Nitrogen cycle model

The N cycle model during the deposition of the Lower Cambrian sediments in the BST region is shown in Fig. 11(a). Such positive $\delta^{15}N$ values may be caused by one of the following processes in the marine N cycle:

(1) Partial nitrification can attract light NO_3^- and heavy residual NH_4^+. Under the premise of complete denitrification of nitrate, the quantitative assimilation of NH_4^+ enriched with ^{15}N by biomass will lead to positive nitrogen isotope bias in sediments. This situation is rarely found, and the cycle will cause an isotopic imbalance with evidence of a large scatter of positive $\delta^{15}N$ excursion in sediments (Chen et al., 2019), which is inconsistent with the characteristics of the BST oils in this study. Thus, partial nitrification may not explain the heavy $\delta^{15}N$ of BST oils.
(2) Incomplete denitrification or anammox occurs in physically stratified systems. The presence of the physically stratified system in the Tarim Basin during the Early Cambrian has been widely reported (Shang et al., 2020; Zhang et al., 2020). The large-scale transgression, volcanism and associated hydrothermal activities enhanced the reducibility of water column (Zhang et al., 2020). The upwelling provided abundant nutrients to the euphotic zone, which further improved the paleoproductivity and increased the consumption of oxygen (Zhu et al., 2016; Zhang et al., 2020). The vertical range in the redox transition zone was expanded, resulting in the better preservation of OM. In this strongly stratified ocean, it is difficult to support a stable NO_3^- pool (Wang et al., 2018), which suggests that the isotope fractionation of denitrification is weakened. On the other hand, the upwelling brings deep NH_4^+ into the redox transition zone and promotes the occurrence of anammox (Wang et al., 2018; Chen et al., 2019). In this process, N is lost from the system in the form of light isotopically enriched N_2, causing the enrichment of ^{15}N in residual NH_4^+, and then it is assimilated by organisms. Therefore, the anammox in the redox transition zone may predominate the heavy $\delta^{15}N$ of BST oils.

Fig. 11(b) presents the N cycle model during the deposition of Middle–Upper Ordovician source rocks in the HLHT region. With

the relative fall in sea level, the increase in surface water oxygenation promoted the reproduction of planktonic algae, reduced the transparency of water column, and limited the survival of benthic algae. The preservation of large phytoplankton meant that the redox interface was shallow. In addition, upwelling was pervasive during the Middle–Late Ordovician, which increased the vertical mixture of chemocline, enlarged the NO_3^- pool, and modulated the redox conditions of mixed area (Ader et al., 2014). In the photic zone, the NO_3^- pool was sufficient, and aquatic organisms obtained N via N-fixation and the assimilation of NO_3^-. NH_4^+ was generated by the mineralization of org-N after the death of organisms, and then undergone complete nitrification, followed by limited denitrification in the mixed area. Furthermore, the deep NH_4^+ was brought into the shallow layer through upwelling, which improved the occurrence of anammox. Unlike the physically stratified system of the Early Cambrian period, the range of the suboxic zone was limited during the Middle–Late Ordovician, and the possibility of biological absorption of ^{15}N-nitrate was decreased due to the sufficient nitrate pool in the surface layer, which resulted in an insignificant positive bias of nitrogen isotope.

6. Conclusions

The $\delta^{15}N$ values of different nitrogenous components (NSOs and asphaltenes) in crude oils reveal the mechanism of isotope fractionation during thermal evolution and provide the following key insights into the compositions of original biomass and environmental characteristics:

(1) The $\delta^{15}N_{Asp}$ values are generally heavier than the $\delta^{15}N_{NSOs}$ values in the marine crude oils from the Tarim Basin, which may result from N transfer and kinetic isotope fractionation during the thermal evolution of OM.
(2) The $\delta^{15}N_{Asp}$ value has a good response to variations in biomass composition and is less affected by sedimentary environment, indicating that it is a reliable indicator for revealing the differences in biological characteristics. The $\delta^{15}N_{NSOs}$ value has a stronger correlation with the redox condition than biological characteristics, and is considered to have a good response to paleoenvironmental variation. These provide a new insight for the study of OM and sedimentary environment of post-over maturity crude oils and corresponding source rocks.
(3) Different N cycles present during the deposition of Lower Cambrian and Middle–Upper Ordovician sediments. In the physically stratified system of the Early Cambrian, anammox occurs with significant isotope fractionation in the redox transition zone, resulting in the heavy $\delta^{15}N$ of OM. In the water column with increased oxygen content of the Middle–Late Ordovician period, due to limitations in the suboxic zone, the enrichment of ^{15}N in organisms caused by partial denitrification is not as significant as that in the Early Cambrian period. The assessment of $\delta^{15}N$ in nitrogenous fractions can contribute to reconstruct a more comprehensive N cycle for ancient oceans.

CRediT authorship contribution statement

Yang Bai: Writing – review & editing, Writing – original draft, Visualization, Methodology, Investigation, Data curation, Conceptualization. **Jian-Fa Chen:** Writing – review & editing, Supervision, Resources, Project administration, Funding acquisition, Conceptualization. **Wen-Zhe Gang:** Writing – review & editing, Supervision, Investigation. **Xin-Jian Zhu:** Supervision, Resources, Project administration, Conceptualization. **Václav Suchý:** Writing – review & editing, Resources. **Shuai-Qi Tang:** Writing – review & editing, Investigation. **Jin Wu:** Writing – review & editing, Investigation. **Min Li:** Writing – review & editing, Investigation. **Sheng-Bao Shi:** Writing – review & editing, Investigation.

Declaration of competing interest

The authors declare that they have no known competing financial interests or personal relationships that could have appeared to influence the work reported in this paper.

Acknowledgements

This work was financially supported by the National Natural Science Foundation of China (No. 41972127) and the National Key Research and Development Program of China (No. 2021YFA0719000). Technical support was provided by the National Key Laboratory of Petroleum Resources and Engineering at the China University of Petroleum, Beijing, China.

References

Ader, M., Cartigny, P., Boudou, J.P., et al., 2006. Nitrogen isotopic evolution of carbonaceous matter during metamorphism: Methodology and preliminary results. Chem. Geol. 232, 152–169. https://doi.org/10.1016/j.chemgeo.2006.02.019.
Ader, M., Sansjofre, P., Halverson, G.P., et al., 2014. Ocean redox structure across the Late Neoproterozoic Oxygenation Event: a nitrogen isotope perspective. Earth Planet Sci. Lett. 396, 1–13. https://doi.org/10.1016/j.epsl.2014.03.042.
Ader, M., Thomazo, C., Sansjofre, P., et al., 2016. Interpretation of the nitrogen isotopic composition of Precambrian sedimentary rocks: assumptions and perspectives. Chem. Geol. 429, 93–110. https://doi.org/10.1016/j.chemgeo.2016.02.010.
Altabet, M.A., Francois, R., 1994. Sedimentary nitrogen isotopic ratio as a recorder for surface ocean nitrate utilization. Global Biogeochem. Cycles 8, 103–116. https://doi.org/10.1029/93GB03396.
Bandurski, E., 1982. Structural similarities between oil-generating kerogens and petroleum asphaltenes. Energy Sources 6, 47–66. https://doi.org/10.1080/00908318208946021.
Bao, J.P., Zhu, C.S., Wang, Z.F., 2018. Typical end-member oil derived from Cambrian-Lower Ordovician source rocks in the Tarim Basin, NW China. Petrol. Explor. Dev. 45, 1177–1188. https://doi.org/10.1016/S1876-3804(18)30121-6.
Baxby, M., Patience, R.L., Bartle, K.D., 1994. The origin and diagenesis of sedimentary organic nitrogen. J. Petrol. Geol. 2, 211–230. https://doi.org/10.1111/j.1747-5457.1994.tb00127.x.
Behar, F., Lorant, F., Lewan, M., 2008. Role of NSO compounds during primary cracking of a Type II kerogen and a Type III lignite. Org. Geochem. 39, 1–22. https://doi.org/10.1016/j.orggeochem.2007.10.007.
Canfield, D.E., Glazer, A.N., Falkowski, P.G., 2010. The evolution and future of Earth's nitrogen cycle. Science 330, 192–196. https://doi.org/10.1126/science.1186120.
Chang, X.C., Shi, B.B., Han, Z.Z., et al., 2017. C_5–C_{13} light hydrocarbons of crude oils from northern Halahatang oilfield (Tarim Basin, NW China) characterized by comprehensive two-dimensional gas chromatography. J. Petrol. Sci. Eng. 157, 223–231. https://doi.org/10.1016/j.petrol.2017.07.043.
Chen, J., Chen, J.F., Shi, S.B., et al., 2020. The linkage of nitrogen isotopic composition and depositional environment of black mudstones in the Upper Triassic Yanchang Formation, Ordos Basin, northern China. J. Asian Earth Sci. 193, 104308. https://doi.org/10.1016/j.jseaes.2020.104308.
Chen, J., Chen, J.F., Yao, L.P., et al., 2023. Influencing factors and significance of organic and inorganic nitrogen isotopic compositions in lacustrine sedimentary rocks. Geosci. Front. 14, 101501. https://doi.org/10.1016/j.gsf.2022.101501.
Chen, Q.L., Yang, X., Chu, C.L., et al., 2015. Recognition of depositional environment of Cambrian source rocks in Tarim Basin. Oil Gas Geol. 36, 880–887. https://doi.org/10.11743/ogg20150602 (in Chinese with English abstract).
Chen, R.Q., Liu, G.D., Shang, F., et al., 2019a. Nitrogen isotope compositions of the upper triassic chang 7 shale, ordos basin, north China: implications for depositional redox conditions. Mar. Petrol. Geol. 109, 279–290. https://doi.org/10.1016/j.marpetgeo.2019.06.027.
Chen, Y., Diamond, C.W., Stüeken, E.E., et al., 2019b. Coupled evolution of nitrogen cycling and redoxcline dynamics on the Yangtze Block across the Ediacaran-Cambrian transition. Geochem. Cosmochim. Acta 257, 243–265. https://doi.org/10.1016/j.gca.2019.05.017.
Cheng, B., Wang, T.G., Chang, X.C., 2013. Geochemical analysis of mixed oil in the ordovician reservoir of the Halahatang depression, Tarim Basin, China. Chin. J. Geochem. 32, 347–356. https://doi.org/10.1007/s11631-013-0642-2.
Cremonese, L., Shields-Zhou, G., Struck, U., et al., 2013. Marine biogeochemical cycling during the early Cambrian constrained by a nitrogen and organic carbon

isotope study of the Xiaotan section, South China. Precambrian Res. 225, 148–165. https://doi.org/10.1016/j.precamres.2011.12.004.
Cui, J., Wang, T., Li, M., et al., 2013. Oil filling history of the Bashituo oilfield in the Markit slope, SW Tarim Basin, China. Petrol. Sci. 10, 58–64. https://doi.org/10.1007/s12182-013-0250-0.
Delwiche, C.C., Steyn, P.L., 1970. Nitrogen isotope fractionation in soils and microbial reactions. Environ. Sci. Technol. 4, 929–935. https://doi.org/10.1021/es60046a004.
Druzhkova, E.I., 2009. Characteristics of the spatial distribution of nanophytoplankton in the vicinity of the Franz Josef Land in summer. Dokl. Biol. Sci. 427, 378–380. https://doi.org/10.1134/S0012496609040218.
Galimov, E.M., 2006. Isotope organic geochemistry. Org. Geochem. 37, 1200–1262. https://doi.org/10.1016/j.orggeochem.2006.04.009.
Godfrey, L.V., Poulton, S.W., Bebout, G.E., 2013. Stability of the nitrogen cycle during development of sulfidic water in the redox-stratified late Paleoproterozoic Ocean. Geology 41, 655–659. https://doi.org/10.1130/G33930.1.
Grantham, P.J., Wakefield, L.L., 1988. Variations in the sterane carbon number distributions of marine source rock derived crude oils through geological time. Org. Geochem. 12, 61–73. https://doi.org/10.1016/0146-6380(88)90115-5.
Gruber, N., Galloway, J.N., 2008. An Earth-system perspective of the global nitrogen cycle. Nature 451, 293–296. https://doi.org/10.1038/nature06592.
Guo, Y., Yu, M.H., Li, Z.Y., et al., 2021. Structural characteristics and hydrocarbon accumulation in Bashituo area, Tarim Basin. Glob. Geol. 24, 154–159. https://doi.org/10.3969/j.issn.1673-9736.2021.03.03.
Hoering, T.C., Moore, H.E., 1958. The isotopic composition of the nitrogen in natural gases and associated crude oils. Geochem. Cosmochim. Acta 13, 225–232. https://doi.org/10.1016/0016-7037(58)90024-3.
Hu, G., Liu, W.H., Borjigin, T., et al., 2014. Tectonic-sedimentary constrains for hydrocarbon generating organism assemblage in the Lower Cambrian argillaceous source rocks, Tarim Basin. Oil Gas Geol. 35, 685–695. https://doi.org/10.11743/ogg20140514 (in Chinese with English abstract).
Hu, G., Liu, W.H., Luo, H.Y., et al., 2019. The impaction of original organism assemblages in source rocks on the kerogen carbon isotopic compositions: a case study of the early Paleozoic source rocks in the Tarim Basin, China. Bull. China Soc. Mineral Petrol. Geochem. 38, 902–913. https://doi.org/10.19658/j.issn.1007-2802.2019.38.133 (in Chinese with English abstract).
Hu, S.Z., Wilkes, H., Horsfield, B., et al., 2016. On the origin, mixing and alteration of crude oils in the Tarim Basin. Org. Geochem. 97, 17–34. https://doi.org/10.1016/j.orggeochem.2016.04.005.
Huo, F., Wang, X.Z., Xu, Z.M., et al., 2019. Characteristics and genesis of the Ordovician crude oil in the RePu area, Halahatang sag, Tarim Basin, China. Petrol. Sci. Technol. 37, 581–588. https://doi.org/10.1080/10916466.2018.1558242.
Kędra, M., Cooper, L.W., Zhang, M., et al., 2019. Benthic trophic sensitivity to ongoing changes in Pacific Arctic seasonal sea ice cover – insights from the nitrogen isotopic composition of amino acids. Deep-Sea Res. Pt. II 162, 137–151. https://doi.org/10.1016/j.dsr2.2019.01.002.
Li, J.F., Zhang, Z.Y., Zhu, G.Y., et al., 2020. The origin and accumulation of ultra-deep oil in Halahatang area, northern Tarim Basin. J. Petrol. Sci. Eng. 195, 107898. https://doi.org/10.1016/j.petrol.2020.107898.
Li, M., Luo, Q.Y., Chen, J.F., et al., 2021. Redox conditions and nitrogen cycling in the late ordovician yangtze sea (south China). Palaeogeogr. Palaeoclimatol. Palaeoecol. 567, 110305. https://doi.org/10.1016/j.palaeo.2021.110305.
Li, M.J., Wang, T.G., Lillis, P.G., et al., 2012. The significance of 24-norcholestanes, triaromatic steroids and dinosteroids in oils and Cambrian–Ordovician source rocks from the cratonic region of the Tarim Basin, NW China. Appl. Geochem. 27, 1643–1654. https://doi.org/10.1016/j.apgeochem.2012.03.006.
Li, S.M., Pang, X.Q., Jin, Z.J., et al., 2001. Characteristics of NSO's compounds in sediment and their geochemical significance. Geochimica 30, 347–352. https://doi.org/10.19700/j.0379-1726.2001.04.007 (in Chinese with English abstract).
Liu, J.Q., Li, Z., Wang, X., et al., 2022. Tectonic-fluid evolution of an ultra-deep carbonate reservoir in the southern Halahatang Oilfield area, Tarim Basin, NW China. Mar. Petrol. Geol. 145, 105870. https://doi.org/10.1016/j.marpetgeo.2022.105870.
Liu, W.H., Borjigin, T., Wang, X.F., et al., 2017. New knowledge of hydrocarbon generating theory of organic matter in Chinese marine carbonates. Petrol. Explor. Dev. 44, 159–169. https://doi.org/10.1016/S1876-3804(17)30020-4.
Mcnair, S.A., Chow-Fraser, P., 2003. Change in biomass of benthic and planktonic algae along a disturbance gradient for 24 Great Lakes coastal wetlands. Can. J. Fish. Aquat. Sci. 60, 676–689. https://doi.org/10.1139/f03-054.
Miyake, Y., Wada, E., 1967. The abundance ratio of $^{15}N/^{14}N$ in marine environments. Rec. Oceanogr. Works Jpn. 9, 37–53. https://www.jamstec.go.jp/biogeochem/pdf/Wada_1967.pdf.
Ni, W., Cao, J., Hu, W., et al., 2024. Complex origins of naphthenic oils in the Junggar Basin, China: biodegradation vs. non-biodegradation. J. Asian Earth Sci. 259, 105891. https://doi.org/10.1016/j.jseaes.2023.105891.
Ning, C.Z., Sun, L.D., Zeng, H.L., et al., 2022. Characteristics of collapsed subsurface paleokarst systems and controlling factors of subsurface paleokarst development in the Lianglitage Formation, Halahatang oilfield, Tarim Basin, NW China. Mar. Petrol. Geol. 137, 105488. https://doi.org/10.1016/j.marpetgeo.2021.105488.
Oldenburg, T.B.P., Brown, M., Bennett, B., et al., 2014. The impact of thermal maturity level on the composition of crude oils, assessed using ultra-high resolution mass spectrometry. Org. Geochem. 75, 151–168. https://doi.org/10.1016/j.orggeochem.2014.07.002.
Peters, K.E., Walters, C.C., Moldowan, J.M., 2005. The Biomarker Guide, second ed. Cambridge University Press, United Kingdom.
Pereira, I., de Aguiar, D.V.A., Vasconselos, G., et al., 2019. Fourier transform mass spectrometry applied to petroleomics. Fund. Appl. Fourier. Transform Mass Spectrom 509–528. https://doi.org/10.1016/B978-0-12-814013-0.00016-8.
Powell, T., 1988. Pristane/phytane ratio as environmental indicator. Nature 333, 604. https://doi.org/10.1038/333604a0.
Prado, G.H.C., Rao, Y., de Klerk, A., 2017. Nitrogen removal from oil: a review. Energy Fuels 31, 14–36. https://doi.org/10.1021/acs.energyfuels.6b02779.
Quan, T.M., Adeboye, O.O., 2021. Interpretation of nitrogen isotope profiles in petroleum systems: a review. Front. Earth Sci. 9, 705691. https://doi.org/10.3389/feart.2021.705691.
Quan, T.M., Adigwe, E.N., Riedinger, N., et al., 2013. Evaluating nitrogen isotopes as proxies for depositional environmental conditions in shales: comparing Caney and Woodford Shales in the Arkoma Basin. Oklahoma. Chem. Geol. 360, 231–240. https://doi.org/10.1016/j.chemgeo.2013.10.017.
Quan, T.M., van de Schootbrugge, B., Field, M.P., et al., 2008. Nitrogen isotope and trace metal analyses from the Mingolsheim core (Germany): evidence for redox variations across the Triassic-Jurassic boundary. Global Biogeochem. Cycles 22, GB2014. https://doi.org/10.1029/2007GB002981.
Rashid, Z., Wilfred, C.D., Gnanasundaram, N., et al., 2019. A comprehensive review on the recent advances on the petroleum asphaltene aggregation. J. Petrol. Sci. Eng. 176, 249–268. https://doi.org/10.1016/j.petrol.2019.01.004.
Schimmelmann, A., Lis, G.P., 2010. Nitrogen isotopic exchange during maturation of organic matter. Org. Geochem. 41, 63–70. https://doi.org/10.1016/j.orggeochem.2009.01.005.
Shang, Y.X., Gao, Z.Q., Fan, T.L., et al., 2020. The Ediacaran–Cambrian boundary in the Tarim Basin, NW China: geological data anomalies and reservoir implication. Mar. Petrol. Geol. 111, 557–575. https://doi.org/10.1016/j.marpetgeo.2019.08.032.
Shanmugam, G., 1985. Significance of coniferous rain forests and related organic matter in generating commercial quantities of oil, Gippsland Basin, Australia. AAPG Bull. 69, 1241–1254. https://doi.org/10.1306/AD462BC3-16F7-11D7-8645000102C1865D.
Shi, K.B., Liu, B., Jiang, W.M., et al., 2017. Sedimentary and evolutionary characteristics of sinian in the Tarim Basin. Petrol. Res. 2, 264–280. https://doi.org/10.1016/j.ptlrs.2017.04.004.
Sigman, D.M., Casciotti, K.L., 2009. Nitrogen isotopes in the ocean. Encyclop. Ocean Sci 3, 40–54. https://doi.org/10.1006/rwos.2001.0172.
Silva, S.R.C., Moncioso, N.A.P., Sad, C.M.S., et al., 2020. Preparation of a nitrogen oil compound fraction by modified gel silica column chromatography. Energy Fuels 34, 5652–5664. https://doi.org/10.1021/acs.energyfuels.0c00266.
Sinninghe Damste, J.S., Kenig, F., Koopmans, M.P., et al., 1995. Evidence for gammacerane as an indicator of water column stratification. Geochem. Cosmochim. Acta 59, 1895–1900. https://doi.org/10.1016/0016-7037(95)00073-9.
Song, D.F., Li, M.J., Shi, S.B., et al., 2019. Geochemistry and possible origin of crude oils from Bashituo oil field, Tarim Basin. AAPG Bull. 103, 973–995. https://doi.org/10.1306/10031817403.
Stüeken, E.E., Kipp, M.A., Koehler, M.C., et al., 2016. The evolution of Earth's biogeochemical nitrogen cycle. Earth Sci. Rev. 160, 220–239. https://doi.org/10.1016/j.earscirev.2016.07.007.
Su, J., Fang, Y., Ma, S.H., et al., 2020. The excursion of nitrogen and carbon isotope in the Lower Cambrian of Tarim Basin: implication for the transformation of anaerobic and euxinic settling. IOP Conf. Ser. Earth Environ. Sci. 600, 012025. https://doi.org/10.1088/1755-1315/600/1/012025.
Sweeney, R.E., Kaplan, I.R., 1980. Natural abundances of ^{15}N as a source indicator for near-shore marine sedimentary and dissolved nitrogen. Mar. Chem. 9, 81–94. https://doi.org/10.1016/0304-4203(80)90062-6.
Tang, Y.J., Li, M.J., Fang, R.H., et al., 2019. Geochemistry and origin of ordovician oils in the rewapu block of the Halahatang oilfield (NW China). Petrol. Sci. 16, 1–13. https://doi.org/10.1007/s12182-018-0284-4.
Tao, S.Z., Wang, C.Y., Du, J.G., et al., 2015. Geochemical application of tricyclic and tetracyclic terpanes biomarkers in crude oils of NW China. Mar. Petrol. Geol. 67, 460–467. https://doi.org/10.1016/j.marpetgeo.2015.05.030.
Ten Haven, H.L., De Leeuw, J.W., Rullkötter, J., et al., 1987. Restricted utility of the pristane/phytane ratio as a palaeoenvironmental indicator. Nature 330, 641–643. https://doi.org/10.1038/330641a0.
Tissot, B.P., Welte, D.H., 1984. Petroleum Formation and Occurrence. Springer-Verlag, Berlin, Germany, pp. 1–699. https://doi.org/10.1016/0012-8252(80)90071-9.
Tyrrell, T., 1999. The relative influences of nitrogen and phosphorus on oceanic primary production. Nature 400, 525–531. https://doi.org/10.1038/22941.
Volkman, J., 2003. Sterols in microorganisms. Appl. Microbiol. Biotechnol. 60, 495–506. https://doi.org/10.1007/s00253-002-1172-8.
Wang, D., Struck, U., Ling, H., et al., 2015. Marine redox variations and nitrogen cycle of the early Cambrian southern margin of the Yangtze Platform, South China: evidence from nitrogen and organic carbon isotopes. Precambrian Res. 267, 209–226. https://doi.org/10.1016/j.precamres.2015.06.009.
Wang, X.Q., Jiang, G.Q., Shi, X.Y., et al., 2018. Nitrogen isotope constraints on the early Ediacaran ocean redox structure. Geochem. Cosmochim. Acta 240, 220–235. https://doi.org/10.1016/j.gca.2018.08.034.
Waples, D.W., Sloan, J.R., 1980. Carbon and nitrogen diagenesis in deep sea sediments. Geochem. Cosmochim. Acta 44, 1463–1470. https://doi.org/10.1016/0016-7037(80)90111-8.
Wei, W., Lu, Y.C., Ma, Y.Q., et al., 2021. Nitrogen isotopes as paleoenvironmental proxies in marginal-marine shales, Bohai Bay Basin, NE China. Sediment. Geol. 421, 105963. https://doi.org/10.1016/j.sedgeo.2021.105963.

Williams, L.B., Ferrell, R.E., Hutcheon, I., et al., 1995. Nitrogen isotope geochemistry of organic matter and minerals during diagenesis and hydrocarbon migration. Geochem. Cosmochim. Acta 59, 765–779. https://doi.org/10.1016/0016-7037(95)00005-K.

Wu, J., Fang, P., Wang, X.C., et al., 2020. The potential occurrence modes of hydrocarbons in asphaltene matrix and its geochemical implications. Fuel 278, 118233. https://doi.org/10.1016/j.fuel.2020.118233.

Wu, Q.Y., Wang, R.Y., Dai, J.B., et al., 1999. Hydrocarbons pyrolysed from nannoplanktonic algae: an experimental organism system for study on the origin of petroleum and natural gas. Chin. Sci. Bull. 44, 767–768. https://doi.org/10.11781/sysydz200903287.

Xia, L.W., Cao, J., Bian, L.Z., et al., 2022. Co-evolution of paleo-environment and bio-precursors in a Permian alkaline lake, Mahu mega-oil province, Junggar Basin: implications for oil sources. Sci. China Earth Sci. 65, 462–476. https://doi.org/10.1007/s11430-021-9861-4.

Xiao, H., Li, M.J., Liu, J.G., et al., 2019. Oil-oil and oil-source rock correlations in the Muglad Basin, Sudan and South Sudan: new insights from molecular markers analyses. Mar. Petrol. Geol. 103, 351–365. https://doi.org/10.1016/j.marpetgeo.2019.03.004.

Yang, S.C., Hu, W.X., Wang, X.L., et al., 2021. Nitrogen isotope evidence for a redox-stratified ocean and eustasy-driven environmental evolution during the Ordovician–Silurian transition. Global Planet. Change 207, 103682. https://doi.org/10.1016/j.gloplacha.2021.103682.

Zhang, C.Y., Guan, S.W., Wu, L., et al., 2020a. Depositional environments of early Cambrian marine shale, northwestern Tarim Basin, China: implications for organic matter accumulation. J. Petrol. Sci. Eng. 194, 107497. https://doi.org/10.1016/j.petrol.2020.107497.

Zhang, J.K., Cao, J., Xia, L.W., et al., 2020b. Investigating biological nitrogen cycling in lacustrine systems by FT-ICR-MS analysis of nitrogen-containing compounds in petroleum. Palaeogeogr. Palaeoclimatol. Palaeoecol. 556, 109887. https://doi.org/10.1016/j.palaeo.2020.109887.

Zhang, S.C., Gao, Z.Y., Li, J.J., et al., 2012. Identification and distribution of marine hydrocarbon source rocks in the Ordovician and Cambrian of the Tarim Basin. Petrol. Explor. Dev. 39, 305–314. https://doi.org/10.1016/S1876-3804(12)60046-9.

Zhang, S.C., Huang, H.P., 2005. Geochemistry of Palaeozoic marine petroleum from the Tarim Basin, NW China: Part 1. Oil family classification. Org. Geochem. 36, 1204–1214. https://doi.org/10.1016/j.orggeochem.2005.01.013.

Zhu, G.Y., Chen, F.R., Chen, Z.Y., et al., 2016. Discovery and basic characteristics of high-quality source rocks found in the Yuertusi Formation of the Cambrian in Tarim Basin, China. J. Nat. Gas Geosci. 1, 21–33. https://doi.org/10.1016/j.jnggs.2016.05.002.

Zhu, G.Y., Milkov, A.V., Zhang, Z.Y., et al., 2019a. Formation and preservation of a giant petroleum accumulation in superdeep carbonate reservoirs in the southern Halahatang oil field area, Tarim Basin, China. AAPG Bull. 103, 1703–1743. https://doi.org/10.1306/11211817132.

Zhu, G.Y., Zhang, Z.Y., Zhou, X.X., et al., 2019b. The complexity, secondary geochemical process, genetic mechanism and distribution prediction of deep marine oil and gas in the Tarim Basin, China. Earth Sci. Rev. 198, 102930. https://doi.org/10.1016/j.earscirev.2019.102930.